A Study of Rice Fissuring by Finite–Element Simulation of Internal Stresses Combined with High–Speed Microscopy Imaging of Fissure Appearance

C.–C. Jia, W. Yang, T. J. Siebenmorgen, R. C. Bautista, A. G. Cnossen

Abstract. *Finite–element analysis was performed to simulate stress distributions inside a rice kernel during drying. The distributions of radial, axial, tangential, and shear stresses were mapped and analyzed. It was found that during drying, two distinct stress zones existed inside a rice kernel: a tensile zone near the surface, and a compressive zone close to the center. Although as drying proceeded, radial, tangential, shear, and axial stresses all decreased in magnitude after they peaked, the first three (i.e., radial, tangential, and shear) stresses approached zero in magnitude and became neutral (i.e., neither tensile nor compressive) after 60 min of drying at 60° C, 17% relative humidity (RH). Only axial stress remained at a pronounced level even after 60 min of drying at 60° C, 17% RH, which helps explain why most fissures form perpendicular to the longitudinal axis of rice kernels. The results were well supported by the fissure appearance caught in this study with high–speed microscopy imaging and by other evidences on rice fissuring published in the literature.*

Keywords. *Rice, Fissuring, Cracking, Fissures, Internal stresses, Drying, Numerical simulation, High–speed imaging.*

The ultimate goal of the rice industry is to produce high–quality rice. To achieve such a goal, artificial drying is typically necessary to prevent microbial spoilage in freshly harvested, high MC (moisture content) rice. During drying, moisture and temperature changes are usually concurrent, which may induce a complicated stress pattern within the kernels. Internal stresses formed within a rice kernel during the drying process may cause an initiation or nucleation of fissures or cracks, if the stresses exceed the material strength, and the nucleation may propagate in a subsequent process following drying when conditions permit. Internal fissures or cracks can lead to kernel breakage during milling and, accordingly, a reduction in rice quality and its market value.

Over the past decades, substantial experimental work has been reported to examine the cause of fissures. Kobayashi et al. (1972) concluded that rice cracking during drying was the result of complex strains caused by moisture content gradients (MCGs) in rice kernels. Yang et al. (2000a) determined the MCGs vs. drying durations by finite–element modeling and examined the relationship of MCGs to the trend of head rice yield, a widely used parameter to judge the severity of breakage of rice kernels. They found that head rice yield was highly related to MCGs. Around the time when MCGs peaked, head rice yield started to suffer a dramatic decrease if rice was cooled immediately and no tempering was performed following drying.

Arora et al. (1973) recognized that rice kernels would experience stresses due to a temperature gradient as well as a moisture content gradient during drying, but the moisture content gradient had more effect on rice fissuring. Muthukumarappan et al. (1992) reported that the volumetric change of rough, brown, and milled rice was linearly related to changes in moisture content and temperature. Some regression models were developed to estimate the volumetric change of rough, brown, and milled rice due to combined changes in MC and temperature of kernels. Kunze and Wratten (1985) and Yamaguchi et al. (1985) reported that rice kernels could be modeled as linear viscoelastic materials. Some empirical formulas were presented to describe the physical and mechanical properties of rice kernels based on experimental studies. Cnossen and Siebenmorgen (2000), Cnossen et al. (2000a, 2000b), Perdon (1999), and Yang et al. (2000a) used the glass transition temperature (Tg) and the differences in material properties above and below Tg to explain fissure formation in rice kernels. They found that the Tg played an important role in rice fissure formation during a desorptive process.

The stress pattern in a rice kernel during drying is a very complex, physically unobservable phenomenon. It is currently impossible to directly determine the internal stress distribution in individual kernels caused by temperature and moisture content changes (Haghighi and Segerlind, 1988a, 1988b; Irudayaraj and Haghighi, 1993; Jia et al., 2000a; Lague and Jenkins, 1991). This being the case, a numerical simulation technique has been used to understand the intra–kernel stress situation. There is limited published

Article was submitted for review in April 2001; approved for publication by the Food & Process Engineering Institute of ASAE in February 2002.

Approved for publication by the University of Arkansas Agricultural Experiment Station.

The authors are **Canchun Jia**, **ASAE Member**, Research Associate, **Wade Yang**, **ASAE Member Engineer**, Research Assistant Professor, **Terry J. Siebenmorgen**, **ASAE Member Engineer**, Professor, **Rustico C. Bautista**, **ASAE Member**, Research Associate, and **Auke G. Cnossen**, Research Specialist, Department of Food Science, University of Arkansas, Fayetteville, Arkansas. **Corresponding author**: Wade Yang, Department of Food Science, University of Arkansas, 2650 N. Young Ave., Fayetteville, AR 72704; phone: 501–575–4678; fax: 501–575–6936; e–mail: wyang@uark.edu.

information on the simulation of stress within rice kernels during drying, especially in regard to the interaction of temperature and MC during drying on stress distribution.

The objectives of this research were to:

1. Develop a finite–element model to predict the internal stresses of rice kernels during the drying process.
2. Infer and analyze possible fissuring patterns in rice kernels based on the simulated stress distributions.
3. Compare the inferred fissuring patterns with high–speed imaging of fissure appearance, as well as with published observations, to validate the finite–element simulations.

FINITE–ELEMENT ANALYSIS OF STRESSES

Brown rice was used in this study to facilitate the direct observation of fissure appearance under a high–speed microscopy imaging system. It is difficult to view fissure occurrence in the endosperm of rough rice. Because of this, finite–element modeling of internal stresses was also performed on brown rice. It was assumed that a brown rice kernel is an elliptical body consisting of two parts (i.e., bran and endosperm). During drying, no external forces are applied to the kernels, and the kernel surface is free to expand or contract.

HYGROSCOPIC AND THERMAL STRAINS

During drying, expansion or contraction occurs due to temperature and moisture content change within a grain kernel. A general assumption for the non–linear thermal–hygroscopic stress problem is based on the linear relationship between strain and the change in temperature and moisture content (Hammerle, 1972). Therefore, if the thermal expansion coefficient of a rice kernel is α, then the thermal strain of the kernel is:

$$\varepsilon_T = \alpha \Delta T \tag{1}$$

where ΔT is temperature gradient. By analogy, the hygroscopic strain of the kernel, with the hygroscopic contraction coefficient of β, can be expressed as:

$$\varepsilon_M = \beta \Delta M \tag{2}$$

where ΔM is moisture content gradient. The constitutive equations and the finite–element approach for obtaining ΔT and ΔM in equations 1 and 2 have been discussed in detail by Jia et al. (2000b) and Yang et al. (2000b). The only difference is that this study used brown rice (a 2–layer model), while those studies used rough rice (a 3–layer model).

NODAL DISPLACEMENTS AND STRAINS

A brown rice kernel may be discretized with axisymmetric linear triangular elements. The coordinate values of these three nodes are (r_i, z_i), (r_j, z_j), and (r_m, z_m). The nodal displacement components (i.e., shrinkage) of an element are (u_i, v_i), (u_j, v_j), and (u_m, v_m) in a cylindrical coordinate system. They are governed by moisture loss and forces exerted by adjacent shells. It was assumed that the nodal displacements along the r and z axes are the linear function of the coordinate. The nodal displacement matrix $\{U\}^e$ of element can be written as:

$$\{U\}^e = \{u \quad v\} = \{\varphi_1 + \varphi_2 r + \varphi_3 z \quad \varphi_4 + \varphi_5 r + \varphi_6 z\} \tag{3}$$

The displacement components (u and v) can be expressed by the element nodal coordinate:

$$u_i = \varphi_1 + \varphi_2 r_i + \varphi_3 z_i, \quad v_i = \varphi_4 + \varphi_5 r_i + \varphi_6 z_i \tag{4}$$

$$u_j = \varphi_1 + \varphi_2 r_j + \varphi_3 z_j, \quad v_j = \varphi_4 + \varphi_5 r_j + \varphi_6 z_j \tag{5}$$

$$u_m = \varphi_1 + \varphi_2 r_m + \varphi_3 z_m, \quad v_m = \varphi_4 + \varphi_5 r_m + \varphi_6 z_m \tag{6}$$

Combining the above equations gives:

$$\begin{Bmatrix} \varphi_1 \\ \varphi_2 \\ \varphi_3 \end{Bmatrix} = \frac{1}{2S} \begin{bmatrix} a_i & a_j & a_m \\ b_i & b_j & b_m \\ c_i & c_j & c_m \end{bmatrix} \begin{Bmatrix} u_i \\ u_j \\ u_m \end{Bmatrix} \tag{7}$$

$$\begin{Bmatrix} \varphi_4 \\ \varphi_5 \\ \varphi_6 \end{Bmatrix} = \frac{1}{2S} \begin{bmatrix} a_i & a_j & a_m \\ b_i & b_j & b_m \\ c_i & c_j & c_m \end{bmatrix} \begin{Bmatrix} v_i \\ v_j \\ v_m \end{Bmatrix} \tag{8}$$

where

$$S = \frac{1}{2}(b_i c_j - b_j c_i)$$

$$a_i = r_j z_m - r_m z_j, \quad b_i = z_j - z_m, \quad c_i = r_m - r_j$$

$$a_j = r_m z_i - r_i z_m, \quad b_j = z_m - z_i, \quad c_j = r_i - r_m$$

$$a_m = r_i z_j - r_j z_i, \quad b_m = z_i - z_j, \quad c_m = r_j - r_i$$

Substituting equations 7 and 8 into equation 3 and re–writing in a matrix form, we have:

$$\begin{Bmatrix} u \\ v \end{Bmatrix} = \begin{Bmatrix} N_i u_i + N_j u_j + N_m u_m \\ N_i v_i + N_j v_j + N_m v_m \end{Bmatrix}$$

$$= \begin{bmatrix} N_i & 0 & N_j & 0 & N_m & 0 \\ 0 & N_i & 0 & N_j & 0 & N_m \end{bmatrix} \begin{Bmatrix} u_i \\ v_i \\ u_j \\ v_j \\ u_m \\ v_m \end{Bmatrix} = [N]\{U\}^e \tag{9}$$

where

$$N_l = \frac{(a_l + b_l r + c_l z)}{2S} \qquad (l = i, j, m)$$

A fundamental difference exists between axisymmetric and plane strains; a fourth component of the strain ($\varepsilon_{\theta\theta}$) must be explicitly considered in addition to the other three strains ($\varepsilon_{\varrho\varrho}$, $\varepsilon_{\zeta\zeta}$, and $\varepsilon_{\varrho\zeta}$). The circumferential strain at a point within the axisymmetric body is caused by the radial displacement (u) at the same point. Therefore, the strain vector (ε) has four components and is defined by:

$$\{\varepsilon\} = \{\varepsilon_{rr} \quad \varepsilon_{\theta\theta} \quad \varepsilon_{zz} \quad \gamma_{rz}\}^T = \left\{\frac{\partial u}{\partial r} \quad \frac{u}{r} \quad \frac{\partial v}{\partial z} \quad \frac{\partial u}{\partial z} + \frac{\partial v}{\partial r}\right\}^T \tag{10}$$

Substituting equation 9 into equation 10 and simplifying:

$$\{\varepsilon\} = [B]\{U\}^e \tag{11}$$

where [B] is as shown in equation 11a

$$[B]=$$

$$\frac{1}{2S}\begin{bmatrix} b_i & 0 & b_j & 0 & b_m & 0 \\ \frac{a_i+b_i\bar{r}+c_i\bar{z}}{\bar{r}} & 0 & \frac{a_j+b_j\bar{r}+c_j\bar{z}}{\bar{r}} & 0 & \frac{a_m+b_m\bar{r}+c_m\bar{z}}{\bar{r}} & 0 \\ 0 & c_i & 0 & c_j & 0 & c_m \\ c_i & b_i & c_j & b_j & c_m & b_m \end{bmatrix} \quad (11a)$$

and

$$\bar{r}=\frac{r_i+r_j+r_m}{3}$$

$$\bar{z}=\frac{z_i+z_j+z_m}{3}$$

The Strain–stress Relationship

Rice kernels may be regarded as a viscoelastic material. Hammerle (1972) and Christensen (1982) described the constitutive relationship between strain and stress in a cylindrical coordinate system:

$$\sigma(x,t)=\int_0^t G(x,t-t')\frac{\partial}{\partial t'}\varepsilon(x,t')dt' \qquad (x=r,\theta,z) \qquad (12)$$

Viscoelastic material properties are highly dependent on temperature and moisture content changes. Hammerle and Mohsenin (1970) suggested that this dependence must be incorporated into the above viscoelastic module. Therefore, the concept of time equivalence of temperature and moisture content effects was put forward. Based on this principle, the shifting procedure for constant temperature states (Christensen, 1982) was extended to transient moisture and temperature states by introducing a new variable called reduced or shifted time. Hammerle (1972) defined the reduced time as:

$$\xi=\frac{t}{\zeta} \qquad (13)$$

$$\zeta=\frac{\zeta_M+\zeta_T}{\zeta_M\zeta_T} \qquad (14)$$

By using reduced time to replace real time in equation 12, the effect of transient thermal–hygroscopic change can be incorporated into the stress–strain relationship (Haghighi and Segerlind, 1988a, 1988b; Hammerle, 1972):

$$\sigma(x,t)=\int_0^t G(x,\xi-\xi')\frac{\partial}{\partial t'}[\varepsilon(x,t')-\varepsilon_M(x,t')-\varepsilon_T(x,t')]dt' \qquad (x=r,\theta,z) \qquad (15)$$

Using the matrix form to rewrite the above equations and noting that a thermal–hygroscopic shear strain cannot exist in an isotropic material, we have:

$$\{\sigma\}=\{\sigma_{rr}\ \ \sigma_{\theta\theta}\ \ \sigma_{zz}\ \ \tau_{rz}\}^T=[D]\begin{Bmatrix}\varepsilon_{rr}-\varepsilon_M-\varepsilon_T\\ \varepsilon_{\theta\theta}-\varepsilon_M-\varepsilon_T\\ \varepsilon_{zz}-\varepsilon_M-\varepsilon_T\\ \varepsilon_{rz}\end{Bmatrix} \qquad (16)$$

$$=[D](\{\varepsilon\}-\{\varepsilon_0\})$$

where $D(\xi-\xi')$ is as shown in equation 16a

$$D(\xi-\xi')=$$

$$\begin{bmatrix} K(\xi-\xi')+\frac{4G(\xi-\xi')}{3} & K(\xi-\xi')-\frac{2G(\xi-\xi')}{3} & K(\xi-\xi')-\frac{2G(\xi-\xi')}{3} & 0 \\ K(\xi-\xi')-\frac{2G(\xi-\xi')}{3} & K(\xi-\xi')+\frac{4G(\xi-\xi')}{3} & K(\xi-\xi')-\frac{2G(\xi-\xi')}{3} & 0 \\ K(\xi-\xi')-\frac{2G(\xi-\xi')}{3} & K(\xi-\xi')-\frac{2G(\xi-\xi')}{3} & K(\xi-\xi')+\frac{4G(\xi-\xi')}{3} & 0 \\ 0 & 0 & 0 & G(\xi-\xi') \end{bmatrix} \quad (16a)$$

and

$$\{\varepsilon_0\}=\begin{Bmatrix}\alpha\Delta\bar{T}+\beta\Delta\bar{M}\\ \alpha\Delta\bar{T}+\beta\Delta\bar{M}\\ \alpha\Delta\bar{T}+\beta\Delta\bar{M}\\ 0\end{Bmatrix}=(\alpha\Delta\bar{T}+\beta\Delta\bar{M})\begin{Bmatrix}1\\1\\1\\0\end{Bmatrix}$$

where for a triangle element, $\Delta\bar{T}$ and $\Delta\bar{M}$ can be expressed as:

$$\Delta\bar{T}=\frac{1}{3}(\Delta T_i+\Delta T_j+\Delta T_m),\quad \Delta\bar{M}=\frac{1}{3}(\Delta M_i+\Delta M_j+\Delta M_m)$$

The Principle of Virtual Displacement

The principle of virtual displacements is actually a special case of the more general principle of virtual work in elementary mechanics. When the virtual displacement is negligible and does not affect the original state of the body, the work done by the external forces in the direction of virtual displacement is equal to the total virtual work done by the internal stresses in the whole domain in the direction of the virtual strains. This principle can be expressed mathematically as:

$$\int_{V^e}(\delta\varepsilon)^T\sigma dV=\int_{V^e}(\delta U)^T F_b dV$$

or

$$\left\{\int_{V^e}B^T DBdV\right\}\{U\}^e-\int_{V^e}B^T D\varepsilon_0 dV=\int_{V^e}N^T F_b dV \qquad (17)$$

The Galerkin method was used to solve the boundary value problem mentioned above (Jia et al., 2000b). Both the triangular decomposition and the backward difference methods were applied to optimize this procedure. The final form of equation 17 is:

$$[K]^e[U]^e=[F]^e \qquad (18)$$

Experimental Procedure and Simulation Process

Experiment Design

Thin–Layer Drying

Tests were carried out in a thin–layer drying system in which air conditions were adjusted to desired values by a temperature–relative humidity (RH) control unit (model 150/300 CFM SS Climate Lab–AA). Long–grain brown rice, variety Cypress, was dried under drying air temperatures of 40°C and 60°C, air RH of 15% and 17%, initial moisture content of 20% wet basis (w.b.), and initial temperature of 25°C. Brown rice was prepared by dehulling rough rice with a Satake lab huller. Average moisture contents of three 15 g

rice samples were measured by the oven method (Banaszek and Siebenmorgen, 1993). The moisture kinetics obtained was used to verify the capability of the finite–element models developed by Jia et al. (2000b) and Yang et al. (2000b) and applied to brown rice drying in this study for ΔT and ΔM determination.

High–Speed Microscopy Imaging

The microscopy imaging system used in this study and the procedure of operations were similar to the video microscopy system reported by Bautista et al. (2000). The system consists of a CCD camera installed with a 50× magnification lens inside a controlled–atmosphere chamber, a camera probe and luminance controller (Moritex 803), a high–resolution monitor (Sony HR Trinitron), a video recorder, a photo printer, and a PC with image processor software. A fiber optic light (Fiber Light model 1700, Dolan–Nenner, Inc.) illuminated the rice kernel under investigation with the light directed parallel to the long axis of the kernel. For normal observation, a 12.5 mm CCD camera (Moritex Scopeman MS803) was used. For a sequential capture of fissure appearance, a high–speed camera (Photron, Japan) was used to capture images at a speed of 1000 frames per second, and the images captured were processed using the software developed by Sensors Applications, Inc. Drying air supplied to the rice kernel under investigation was generated in the same air parameter generation and control unit (model 150/300 CFM SS Climate Lab–AA) mentioned earlier.

Simulation Process

An axisymmetric finite–element grid of a quarter cross–section of a single brown rice kernel in cylindrical coordinates is shown in figure 1. Temperature and moisture content were described using unsteady–state modified Luikov equations (Luikov, 1966). The finite–element technique, which divides an elliptical grain kernel into a large number of small triangle elements across a section of the kernel and describes the variation of a field within an element using interpolating polynomials, was applied to solve those equations, as described in detail by Jia et al. (2000b) and Yang et al. (2000b), and ΔT and ΔM were determined accordingly. Thermal and hygroscopic strains were obtained by inserting ΔT and ΔM into equations 1 and 2. These values with related property parameters were substituted into equation 18 to calculate the respective displacements at a given time step. Finally, stresses were obtained from equation 16 by combining equation 11 with equations 1 and 2. This procedure was repeated until the drying process ended.

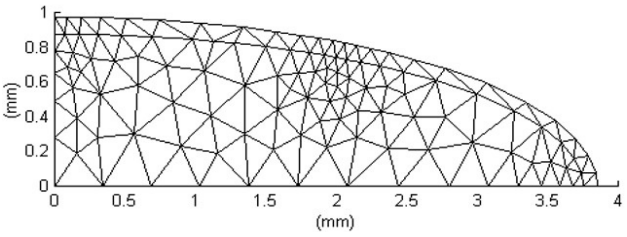

Figure 1. Finite–element mesh for a Cypress (long–grain) brown rice kernel (1/4 cross–section, 123 nodes, and 199 elements).

Coefficients and Viscoelastic Properties for Simulation

The property parameters for the simulation were taken from published literature (Kunze and Wratten, 1985; Yamaguchi et al., 1985):

$$\alpha(t) = 0.00000312 + 0.003657M(t)^2 + 0.01097M(t)^3 \quad (19)$$

$$\beta(t) = \frac{0.3533 + 0.001967(T(t) - 273)}{(1 + (1.06 + 0.0059(T(t) - 273)M(t)))^{\frac{2}{3}}} \quad (20)$$

$$K(t) = 0.667E(t)\left(0.3e^{-\frac{t}{\varsigma_1(t)}} + 0.7e^{-\frac{t}{\varsigma_2(t)}}\right) \quad (21)$$

$$G(t) = 0.4E(t)\left(0.3e^{-\frac{t}{\varsigma_1(t)}} + 0.7e^{-\frac{t}{\varsigma_2(t)}}\right) \quad (22)$$

where

$$E(t) = \frac{1.0\times10^{11}}{M(t)T(t)}$$

$$\varsigma_1(t) = 1.81\times10^5 e^{-A}$$

$$\varsigma_2(t) = 4.32\times10^6 e^{-A}$$

$$\zeta_T(t) = 351e^{-0.02T(t)}$$

$$\zeta_M(t) = 6.49e^{-11M(t)}$$

Results and Discussion

Verification of the Finite–Element Models

Comparison between the simulated and the measured average moisture contents under two different thin–layer drying conditions (i.e., 60° C, 17% RH, and 40° C, 15% RH) is shown in figure 2. It can be seen that the simulated results agreed well with the measured values. This indicates that the finite–element formulas were capable of predicting the brown rice drying process and could be used to accurately obtain ΔT and ΔM for the internal stress analysis.

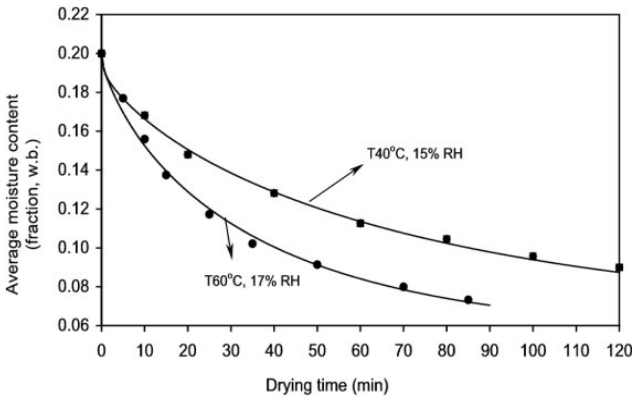

Figure 2. Simulated (curves) and measured (symbols) average moisture contents for a Cypress (long–grain) brown rice kernel at initial moisture content of 20.0% (w.b.) and two different drying conditions (T = drying temperature, RH = drying air relative humidity).

Moisture and Temperature Distributions

Figure 3 shows the moisture content distribution (upper two graphs) inside the rice kernel at two selected times: 15 min and 60 min under drying condition of 60° C and 17% RH. Only a quarter section of the kernel is shown due to the symmetrical assumption of rice kernels. Figure 3 also shows the temperature distribution (lower two graphs) inside the rice kernel at two selected times: 1 min and 5 min under drying condition of 60° C and 17% RH. It was found that the whole kernel reached the drying temperature of 60° C after about 2.5 min. Yang et al. (2000b) reported a similar result for rough rice. In other words, temperature gradients died down completely after the first few minutes of drying. However, moisture content changes were much slower than temperature changes. The moisture content of the outermost layers of the kernel decreased to equilibrium moisture content within a short time, but moisture in the center part of the kernel was still at a relatively high level even after 60 min of drying. Moisture content differences between the center and the surface existed throughout the drying process, but they dropped gradually over time. The results suggested that, during the drying process of rice, the effect of temperature gradients seemed to be much less than that of moisture content gradients, which agreed with the conclusion by Arora et al. (1973).

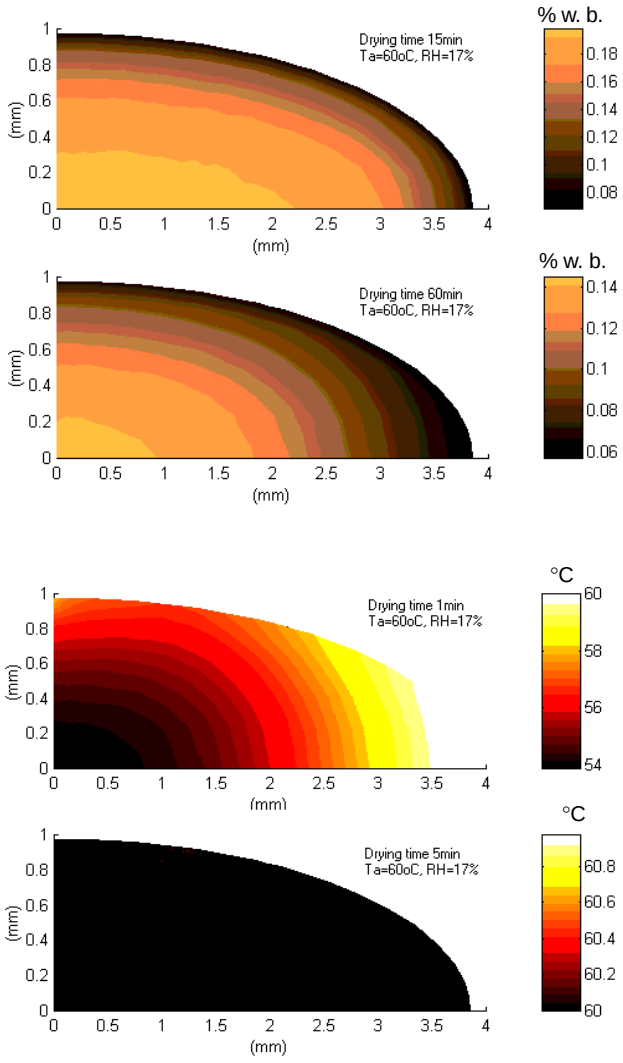

Figure 3. Moisture (upper two graphs) and temperature (lower two graphs) distributions at selected drying times for a Cypress brown rice kernel (1/4 kernel shown) at initial moisture content of 20.0% (w.b.) and equilibrium moisture content (EMC) of 6.0% (w.b.) (Ta = drying temperature, RH = drying air relative humidity).

Stress Distribution and Behavior

Four major stress components (i.e., axial, radial, shear, and tangential stress) were calculated and are analyzed below (figs. 4 to 7). Simulation results are shown, as an example, at two drying durations (15 min and 60 min) and under two drying conditions: 40° C, 15% RH (upper two graphs) and 60° C, 17% RH (lower two graphs). Initial moisture content of the rice was 20% (w.b.). Positive values of stress represent tension, while negative values represent compression. The humidity ratio was 0.022 kg water/kg dry air in the air at 60° C, 17% RH, and 0.009 kg water/kg dry air in the air at 40° C, 15% RH.

Figure 4 shows the radial stress distributions under the two drying conditions mentioned above. Compressive and tensile radial stresses co–existed inside the rice kernel in different locations. There were basically two major stress zones observed inside the kernel: a tensile stress zone closer to the surface, and a compressive stress zone closer to the center. The size of the zones or the location of the zero stress plane (i.e., neutral location, neither compressive nor tensile) varied according to the duration of drying. At 15 min, the tensile zone covered an area, on the surface side, that was approximately 1/3 of the kernel's thickness, and the rest corresponded to the compressive zone closer to the center. As drying proceeded, both compressive and tensile stresses in the two zones gradually reduced their magnitude, after they passed the peak values, and became neutral or stayed slightly tensile (fig. 4). As can be seen from the 60 min graphs in figure 4, the entire kernel almost became one zone, with stresses very close to zero or slightly tensile everywhere except the kernel tip, where the compressive stress was gradually increased with time.

Kunze and Choudhury (1972) explained qualitatively the phenomenon of compressive and tensile zoning, as confirmed in this study. During drying, the outer cells of a kernel shrink as they lose moisture. In order for moisture to transfer from a kernel to the environment, a moisture content gradient, depending mainly on drying temperature and humidity ratio, must exist from the center to the surface of the kernel. Hence, the inner portions of the kernel are at higher moisture content than surface portions. The result is that the surface cells tend to contract, which generates a local tensile stress that must be equilibrated by internal compressive stresses. This phenomenon causes tension at the layers close to surface and compression at the center of the grain. Tension of this type decreases or disappears when the outer moisture of the kernel is next to equilibrium moisture content, and moisture content gradients gradually vanish.

Figure 5 illustrates the simulated axial stress distributions under the two selected drying conditions. Similar to radial stresses, two major zones of compressive and tensile stresses were observed. Each zone occupied a certain area; the tensile zone was close to the surface, and the compressive zone surrounded the center. The axial stresses were higher in magnitude than the radial stresses in either zone, given the same drying time and drying conditions. As drying went on, the stresses in the compressive zone gradually changed

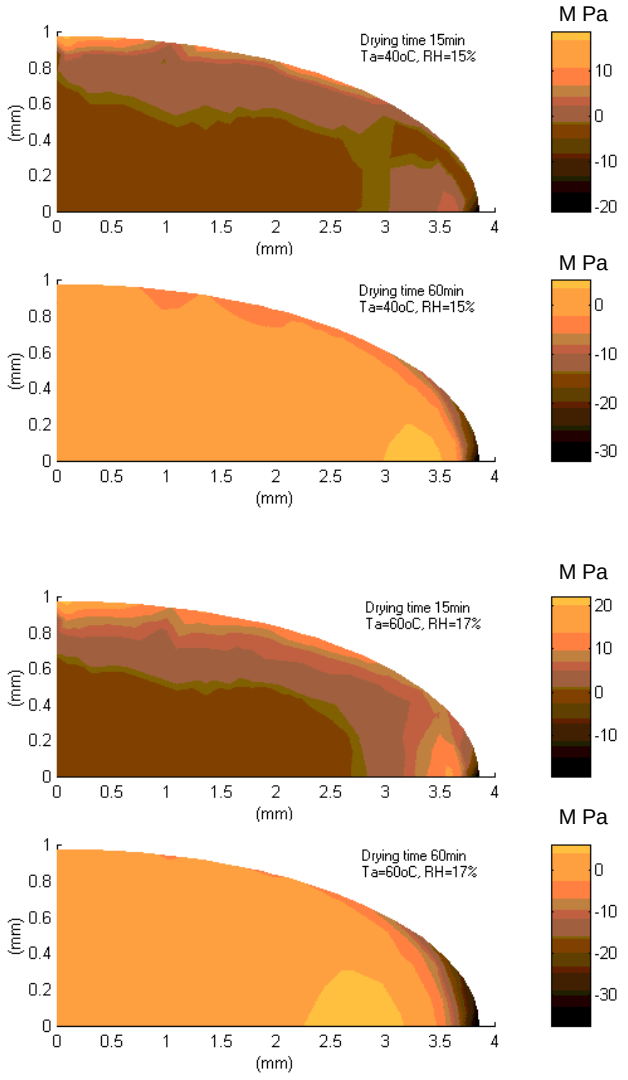

Figure 4. Simulated radial stress ($\sigma_{\theta\theta}$) distributions for a Cypress brown rice kernel (1/4 kernel shown) at initial moisture content of 20.0% (w.b.) and different drying stages (Ta = drying temperature, RH = drying air relative humidity). Positive and negative values are for tensile and compressive stresses, respectively.

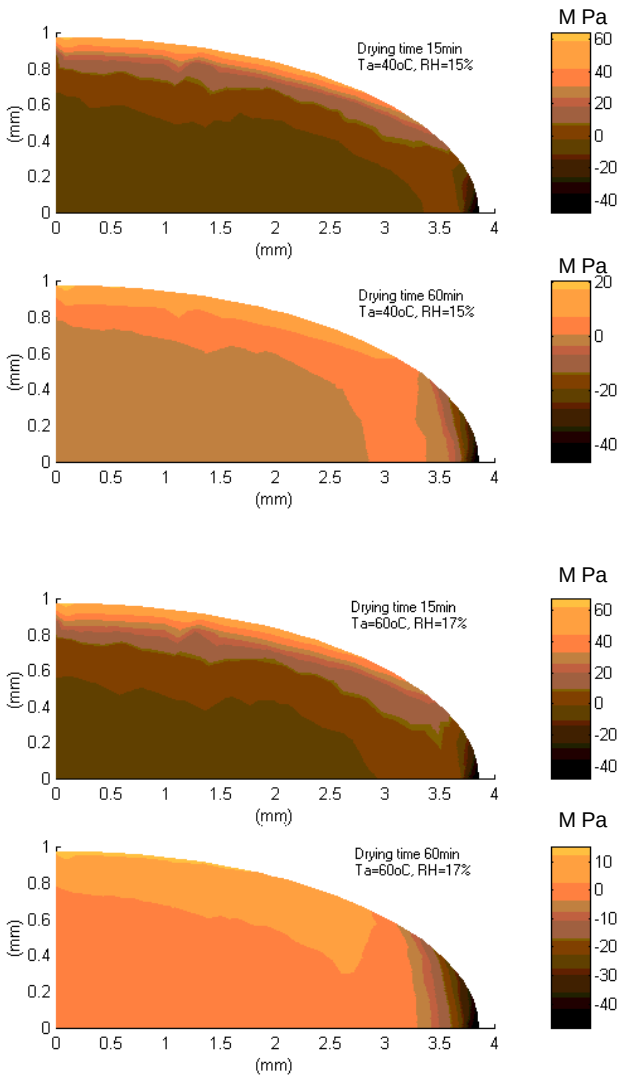

Figure 5. Simulated axial stress ($\sigma_{\xi\xi}$) distributions for a Cypress brown rice kernel (1/4 kernel shown) at initial moisture content of 20.0% (w.b.) and different drying stages (Ta = drying temperature, RH = drying air relative humidity). Positive and negative values are for tensile and compressive stresses, respectively.

magnitude towards neutral or slightly tensile. However, the stresses in the tensile zone remained, although somewhat deceased in magnitude, tensile at a considerable level and covered a certain area next to surface (fig. 5), even after 60 min of drying. As a result, the entire kernel was subjected to tension longitudinally. Similarly, compressive stresses along the axial direction remained strong at the kernel tip.

Shear stresses were negative (i.e., compressive) during drying under all drying conditions. Figure 6 shows the shear stress distributions under the two drying conditions involved in this study. The largest compressive shear stresses were at the surface around the kernel tip. As drying went on, shear stresses move further inside the kernel. Although their magnitude gradually decreased, they remained at a certain level. As can be seen in figure 6, in most regions of the kernel, the magnitude of shear stresses was minimal throughout the drying process, which indicates that the effect of shear stresses on rice fissuring may be insignificant.

Tangential stress distributions are shown in figure 7. The patterns and behavior of the tangential stress distribution were very similar to those of radial stresses, in terms of compressive and tensile zoning and compressive stress concentration around the kernel tip, except that the absolute peak values of tangential stress were greater than those of radial stress. Like radial stresses, the tangential stresses everywhere inside the kernel, except the kernel tip region, also approached neutral after 60 min of drying (fig. 7).

Reflections on Some Rice Fissuring Phenomena

One of the most prominent phenomena of rice fissuring is the development of rice fissures along the radial direction (i.e., perpendicular to the longitudinal axis). Although other forms of fissures have been observed and reported in the literature (Bautista, 1998), the predominant fissures were perpendicular to the longitudinal axis of a kernel, especially a long–grain kernel. Figure 8 shows a series of snapshots of

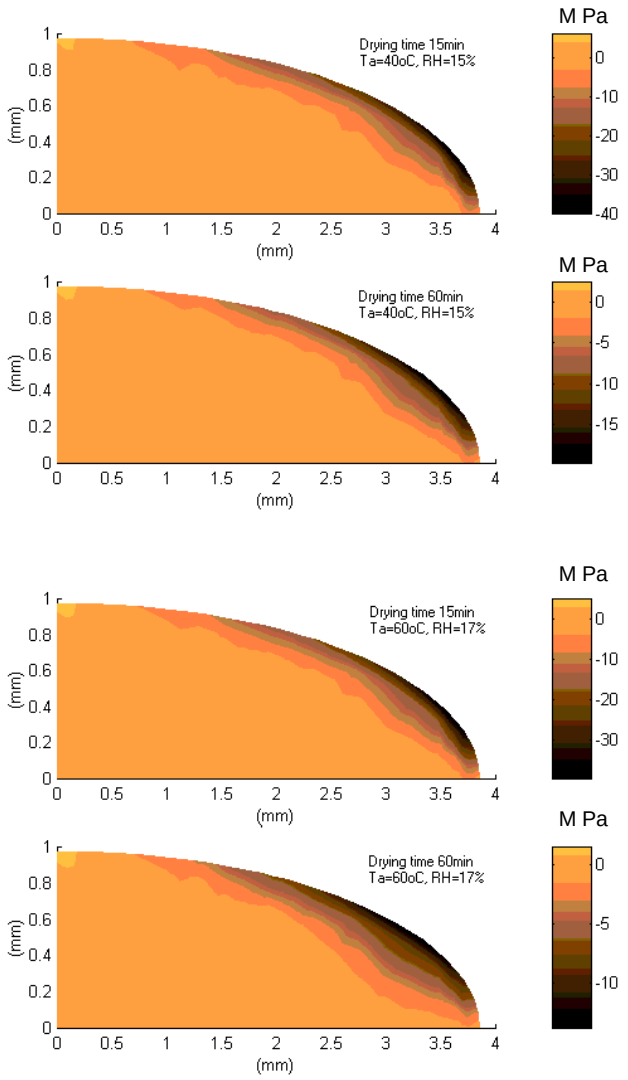

Figure 6. Simulated shear stress ($\tau_{\theta\xi}$) distributions for a Cypress brown rice kernel (1/4 kernel shown) at initial moisture content of 20.0% (w.b.) and different drying stages (Ta = drying temperature, RH = drying air relative humidity). Positive and negative values are for tensile and compressive stresses, respectively.

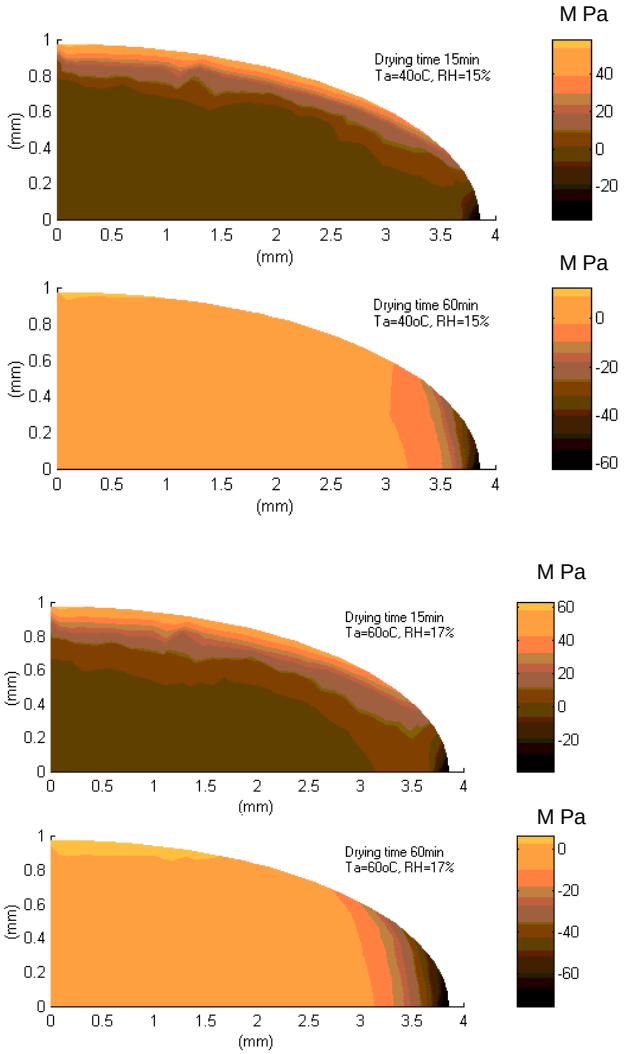

Figure 7. Simulated tangential stress (σθθ) distributions for a Cypress brown rice kernel (1/4 kernel shown) at initial moisture content of 20.0% (w.b.) and different drying stages (Ta = drying temperature, RH = drying air relative humidity). Positive and negative values are for tensile and compressive stresses, respectively.

Figure 8. Occurrence and propagation of a fissure between two existing fissures inside a rice kernel as captured by the high–speed microscopy imaging system. The kernel was dried at 60° C, 20% RH, for 50 min and then naturally cooled in ambient conditions.

a rice kernel taken by the video microscopy system depicting the occurrence and development of a fissure inside a rice kernel in 0.005 s between two fissures that have already developed. The kernel was dried at 60° C, 20% RH, for 50 min and then naturally cooled in ambient conditions for over one hour. From the fissure images recorded at 0.001 s to 0.005 s, it is obvious that the fissure occurred in a region closer to the surface of the kernel on the ventral side. It then worked its way towards the dorsal side at more or less a right angle to the longitudinal axis.

The phenomenon that most fissures are perpendicular to the longitudinal axis can be explained by the pattern of stress distribution inside a rice kernel during drying, as found in this study. As mentioned above, radial, shear, and tangential stresses gradually died down as the drying proceeded. After a sufficient drying duration, these stresses were not significant at all in magnitude and were very close to a neutral state. However, the axial stresses remained considerably strong even after 60 min of drying at 60° C. After a certain drying duration, the axial stresses were basically tensile throughout the kernel, except around the kernel tip, and they were the only significant stresses inside the kernel. When drying stopped, the stress inside the kernel was carried over to subsequent processes. It would remain inside the kernel unless a tempering process was conducted to relieve it. Therefore, any fissure or crack, no matter how tiny, initiated inside the endosperm during or after drying would be likely to propagate vertically because of the tensile effect created inside the kernel. The effect of stresses in other directions was insignificant, as discussed earlier.

CONCLUSIONS

A finite–element model for brown rice drying has been developed and verified by thin–layer drying kinetics. Internal viscoelastic stress distributions in a rice kernel were simulated. The distributions of radial, axial, tangential, and shear stresses were mapped and analyzed. It was found that two distinct stress zones existed inside a rice kernel during drying: a tensile zone that was closer to the surface, and a compressive zone that was closer to the center. It was also found that, as drying proceeded, radial, tangential, and shear stresses gradually approached zero in magnitude and became neutral in direction after 60 min of drying at 60° C, 17% relative humidity. Only axial stress remained at a pronounced level, even after 60 min of drying at 60° C, 17% relative humidity, which helped explain why most fissures propagate perpendicular to the longitudinal axis of rice kernels.

ACKNOWLEDGEMENTS

The authors would like to thank the Arkansas Rice Research and Promotion Board and the corporate sponsors of the University of Arkansas Rice Processing Program for financial support of this research, and the Rice Research and Extension Center in Stuttgart, Arkansas, for supplying the rice for this research.

REFERENCES

Arora, V. K., S. M. Henderson, and T. H. Burkhardt. 1973. Rice drying cracking versus thermal and mechanical properties. *Trans. ASAE* 16(2): 320–327.

Banaszek, M. M., and T. J. Siebenmorgen. 1993. Individual rice kernel drying curves. *Trans. ASAE* 36(2): 521–527.

Bautista, R. C. 1998. Experimental studies on fissure occurrence in rice by desorption and adsorption of moisture. PhD diss. Morioka, Japan: Iwate University.

Bautista, R. C., T. J. Siebenmorgen, and A. G. Cnossen. 2000. Fissure formation characterization in rice kernels using video microscopy. In *Proc.12th International Drying Symposium* IDS2000, Paper No. 417. P. J. A. M. Kerkhof, W. J. Coumans, and G. D. Mooiweer, eds. Noordwijkerhout, The Netherlands. Aug. 28–31. Amsterdam, the Netherlands: Elsevier Science.

Christensen, R. M. 1982. *Theory of Viscoelasticity: An Introduction*. New York, N.Y.: Academic Press, Inc.

Cnossen, A. G., and T. J. Siebenmorgen. 2000. The glass transition temperature concept in rice drying and tempering: Effect on milling quality. *Trans. ASAE* 43(6): 1661–1667.

Cnossen, A. G., T. J. Siebenmorgen, A. A. Perdon, W. Yang, and R. C. Bautista. 2000a. A hypothesis for explaining fissure formation in rice kernels during the drying process. In *Proc.12th International Drying Symposium* IDS2000, Paper No. 63. P. J. A. M. Kerkhof, W. J. Coumans, and G. D. Mooiweer, eds. Noordwijkerhout, The Netherlands. Aug. 28–31. Amsterdam, the Netherlands: Elsevier Science.

Cnossen, A. G., T. J. Siebenmorgen, and W. Yang. 2000b. Incorporating the glass transition temperature to measure rice drying and tempering behavior. ASAE Paper No. 006018. St. Joseph, Mich.: ASAE.

Haghighi, K., and L. J. Segerlind. 1988a. Failure of biomaterials subjected to temperature and moisture gradients using the finite–element method: Part 1. Thermo–hydro viscoelasticity. *Trans. ASAE* 31(3): 930–937.

_____. 1988b. Failure of biomaterials subjected to temperature and moisture gradients using the finite–element method: Part 2. Stress analysis of an isotropic sphere during drying. *Trans. ASAE* 31(3): 938–946.

Hammerle, J. R. 1972. Theoretical analysis of failure in a viscoelastic slab subjected to temperature and moisture gradients. *Trans. ASAE* 15(5): 960–965.

Hammerle, J. R., and N. N. Mohsenin. 1970. Tensile relaxation modulus of corn horny endosperm as a function of time, temperature, and moisture content. *Trans. ASAE* 13(3): 372–375.

Irudayaraj, J., and K. Haghighi. 1993. Stress analysis of viscoelastic material during drying: Part 2. Application to grain kernels. *Drying Technology* 11(5): 929–959.

Jia, C.–C., D.–W. Sun, and C.–W. Cao. 2000a. Mathematical simulation of stresses within a corn kernel during drying. *Drying Technology* 18(4&5): 887–906.

_____. 2000b. Mathematical simulation of temperature and moisture fields within a grain kernel during drying. *Drying Technology* 18(6): 1305–1325.

Kobayashi, H., Y. Miwa, and K. Hayakawa. 1972. On the mechanism of the cracking in rice kernels during drying of paddies, particularly moisture distribution and drying strain in one kernel. *Research Bulletin* 33: 279–293. Gifu, Japan: Gifu University, Faculty of Agriculture.

Kunze, O. R., and M. S. U Choudhury. 1972. Moisture adsorption related to the tensile strength of rice. *Cereal Chemistry* 49(46): 684–696.

Kunze, O. R., and F. T. Wratten. 1985. Physical and mechanical properties of rice. Chapter 5 in *Rice: Chemistry and Technology.* B. O. Juliano, ed. St. Paul, Minn.: American Association of Cereal Chemists.

Lague, C., and B. M. Jenkins. 1991. Modeling pre–harvest stress–cracking of rice kernels: Part 1. Development of a finite–element model. Trans. ASAE 34(4): 1798–1811.

Luikov, A. V. 1966. *Heat and Mass Transfer in Capillary Bodies*. New York, N.Y.: Pergamon Press.

Muthukumarappan, K., V. K. Jindal, and S. Gunasekaran. 1992. Volumetric changes in rice kernels during desorption and adsorption. *Trans. ASAE* 35(1): 235–241.

Perdon, A. A. 1999. Amorphous state transition in rice during the drying process. PhD diss. Fayetteville, Ark.: University of Arkansas.

Yamaguchi, S., K. Wakabarashi, and S. Yamazawa. 1985. Properties of brown rice kernel for calculation of drying stresses. In *Drying '85*, 438–444. New York, N.Y.: Hemisphere Publishing.

Yang, W., C.–C. Jia, T. J. Siebenmorgen, and A. G. Cnossen. 2000a. Intra–kernel moisture gradients and glass transition temperatures in relation to head rice yield variation during heated air drying of rough rice. In *Proc.12th* International Drying Symposium IDS2000, Paper No. 69. P. J. A. M. Kerkhof, W. J. Coumans, and G. D. Mooiweer, eds. Noordwijkerhout, The Netherlands. Aug. 28–31. Amsterdam, the Netherlands: Elsevier Science.

Yang, W., C.–C. Jia, T. J. Siebenmorgen, T. A. Howell, and A. G. Cnossen. 2000b. Intra–kernel moisture and temperature response of rice to drying and tempering treatments by finite–element simulation. ASAE Paper No. 006003. St. Joseph, Mich.: ASAE.

NOMENCLATURE

E = uniaxial tensile relaxation modulus (Pa)
F_b = body force (N)
G = shear relaxation modulus (Pa)
K = bulk relaxation modulus (Pa)
M = moisture content of a single grain kernel (d.b.)
$\overline{M}$ = average moisture content of a single grain kernel (d.b.)
r, z = r and z axes in a cylindrical coordinate system
S = total surface area of a triangular element (m^2)
t = drying time (s)
T = temperature of a single grain kernel (°C)

$\bar{T}$ = average temperature of a single grain kernel (°C)
u, v = element displacement along the r and z axis, respectively (m)

Greek Symbols

α = thermal expansion coefficient (1/°C)
β = hygroscopic contraction coefficient (1/d.b.)
γ = shear strain (m/m)
ε = normal strain (m/m)
ς = relaxation time (s)
ζ = shift factor
ξ = reduced time (s)
σ = normal stress (Pa)
τ = shear stress (Pa)
$\phi_1 - \phi_6$ = constants

Subscripts

i, j, m = three nodes of an element
M = moisture content
T = temperature
rr = radial
zz = axial
rz = shear
$\theta\theta$ = circumferential or tangential